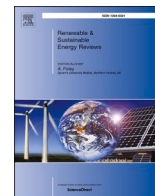


Contents lists available at [ScienceDirect](https://www.sciencedirect.com)

Renewable and Sustainable Energy Reviews

journal homepage: www.elsevier.com/locate/rser

Combined wind-solar electricity production potential over north-western Africa

Imre M. Jánosi^{a,b,*}, Karim Medjdoub^c, Miklós Vincze^{c,d}^a Department of Water and Environmental Policy, Faculty of Water Sciences, University of Public Service, Ludovika tér 2, H-1083, Budapest, Hungary^b Max Planck Institute for the Physics of Complex Systems, Nöthnitzer Str. 38, 01187, Dresden, Germany^c von Kármán Laboratory for Environmental Flows, ELTE Eötvös Loránd University, Pázmány P. stry. 1/a, H-1117, Budapest, Hungary^d MTA-ELTE Theoretical Physics Research Group, Pázmány P. stry. 1/a, H-1117, Budapest, Hungary

ARTICLE INFO

Keywords:

Wind energy
Solar energy
Hybrid wind-solar electricity systems
Spatial and temporal correlations
North-western Africa

ABSTRACT

In this work we analyze wind speed and solar irradiation data of high spatial and temporal resolution for an extended area of north-western Africa including the Mediterranean Sea. We exploit the ERA5 data bank compiled and maintained by the European Centre for Medium Range Weather Forecast (ECMWF). One of the new products they provide is horizontal wind speed components at a height of 100 m (modern wind turbines have a hub height between 80 and 120 m). We demonstrate that the desert area is an optimal location for wind- and solar electricity production for two peculiar aspects. Firstly, the wind speeds at 100 m over the Sahara are almost as large as wind speeds over the open sea. Wind speed differences between the standard 10 m altitude and 100 m level are considerably larger over the desert area than over the sea. Secondly, there are utilizable anti-correlations between local wind speeds at 100 m and surface solar radiations over the Sahara. As far as we know, such anti-correlations over our target area are not considered until very recently as an exploitable source of combined solar-wind electricity production. We provide a theoretically optimum combination of the two resources in a simple model framework. The result is that resource combinations between 60-40% and 70-30% wind-solar electricity aggregation (depending on the geographic location) provide an optimally smooth output with a minimal loss of total production achieved by either pure wind or pure photo-voltaic generation.

1. Introduction

Access to electricity can play a critical role in sustainable development in Africa [1–3]. In September 2015, United Nations member states adopted a comprehensive global development agenda known as the Sustainable Development Goals. The 17 goals cover everything from poverty, hunger, health, education, gender equality, water to climate, peace and justice, among others [4]. Goal 7 entitled “Ensure access to affordable, reliable, sustainable and modern energy for all”, with an emphasis on renewable sources. In the past decade, the population with access to electricity increased by 1 billion people (reaching ~90% of the global population), still around 800 million individuals, mostly living in rural areas, lack this fundamental service [4]. There were promising improvements at several regions, particularly in Latin America and South-Eastern Asia, however the population growth in Africa was faster than the increase of access to electricity. The

development of energy sector, especially the expansion of modern solar and wind resources is hindered by several factors in Africa including the lack of initial capital, lack of skilled workforce, weak maintenance service, poor infrastructure and institutional background, etc. [1,5]. It is a particularly unfortunate fact, because the climate over a large part of the African continent provides excellent opportunities for installing solar and wind electricity facilities, as we will demonstrate also in this study.

The spatial and temporal variability of climate variables and intermittency of renewable electricity sources have a vast literature, for a recent review see Engeland et al. [6]. Somewhat less attention has been paid on combined (the other term is hybrid) solar and wind power systems, however the interest is continuously increasing [7–11]. Complementarity of various renewable resources, such as wind, solar and hydropower, has been studied in all continents, Africa is somewhat underrepresented [7,11]. Suitable geographic locations where wind and solar resources exhibit temporal anti-correlations have been identified

* Corresponding author. Department of Water and Environmental Policy, Faculty of Water Sciences, University of Public Service, Ludovika tér 2, H-1083, Budapest, Hungary. karman3.elte.hu/janosi

E-mail address: janosi.imre.miklos@uni-nke.hu (I.M. Jánosi).

<https://doi.org/10.1016/j.rser.2021.111558>

Received 3 November 2020; Received in revised form 5 July 2021; Accepted 4 August 2021

Available online 1 September 2021

1364-0321/© 2021 The Authors. Published by Elsevier Ltd. This is an open access article under the CC BY license (<http://creativecommons.org/licenses/by/4.0/>).

Table 1

ERA5 variables used in this work. 'Id' refers to the short name of parameters in the ERA5 nomenclature. Note that *ssrd* is an accumulated parameter, mean flux (Wm^{-2}) are obtained by dividing the integration time (3600 s).

Id	long name	units
<i>cvl</i>	Low vegetation cover	[0–1]
<i>cvh</i>	High vegetation cover	[0–1]
<i>u10</i>	10 m u-component (eastward) of wind	ms^{-1}
<i>v10</i>	10 m v-component (northward) of wind	ms^{-1}
<i>u100</i>	100 m u-component (eastward) of wind	ms^{-1}
<i>v100</i>	100 m v-component (northward) of wind	ms^{-1}
<i>ssrd</i>	Surface solar radiation downwards (accum.)	Jm^{-2}

in Australia [12], in the north-eastern part of the Arabian Peninsula (on a monthly time scale) [13], over the European subcontinent when solar and wind power are integrated across Europe [14,15], in Sweden (grid integrated) from hourly to yearly timescales [16], in the Iberian Peninsula [17,18], Argentina [19], China [20] and a couple of other locations (see the literature in the reviews by Jurasz et al. [8], Solomon et al. [9] and Weschenfelder et al. [10]). These studies have been introduced simpler and more complicated measures to characterize complementarity starting from the temporal correlations on various timescales to the more demanding principal component analysis and canonical correlation analysis [18]. Note that temporal complementarity depends on the timescales considered, e.g. it can be present on seasonal or annual scales but it is negligible in hourly or daily intervals [8,21].

In order to estimate wind and solar electricity production potential, we analyze ERA5 reanalysis data of high spatial and temporal resolution over north-western Africa. Figure S1 in the Supplementary Material illustrates our target area which is centered around Algeria, including the Mediterranean Sea. The dominating geographic feature of the region is the Sahara, which lacks surface vegetation almost entirely. Low vegetation refers to crops and mixed farming, irrigated crops, short grass and tall grass in this area (Fig. S1a), while high vegetation (evergreen trees, deciduous trees, mixed forest/woodland, and interrupted forest) is practically present only along the coasts of the Mediterranean Sea and the Atlantic Ocean (Fig. S1b). Data analysis revealed two peculiar features over the Sahara. A comparison of wind speeds at 10 m and 100 m altitudes indicates steep vertical wind profiles over the Sahara, where wind velocities at larger heights are comparable with wind velocities over open sea. This provides an optimal circumstance for on-shore wind electricity generation with capacity factors similar to the off-shore facilities demanding much larger initial capital.

The second peculiarity is observed by evaluating high temporal resolution (1 h) wind and insolation records in the central part of region denoted by a blue rectangle in Fig. S1. Namely, the wind at 100 m altitude is significantly intensified during the nighttime periods over extended regions. This provides an opportunity to integrate wind and solar electricity, where the output is substantially smoother than in the case of either only wind or only solar generation. The most suitable area (centered in In Salah province) is very far from the densely inhabited coastal regions, however as a first step, proper installations can supply the local population (In Salah and Tamanrasset provinces, estimated total population is around 165 thousands inhabitants). For this reason, we do not consider any grid integration issues, we assume distributed energy production.

After submitting our manuscript, a paper appeared by Guezgouz et al. [11] on an analysis of solar and wind energy complementarity in Algeria. We will discuss the differences between our study and Ref. [11] in details in Section 4 (Discussion).

2. Data and methods

ERA5 is the fifth generation ECMWF atmospheric reanalysis of the global climate [22]. It combines model data with global observations

into a complete and consistent gridded ($0.25^\circ \times 0.25^\circ$) dataset on 137 pressure levels spanning the surface of the Earth to 0.01 hPa, from 1979 onward (regularly updated) with a temporal resolution of 1 h (In a preliminary version, ERA5 reanalysis backward extension is available from 1950 to 1978, too.) The time variable assigned to all data is in UTC (Universal Time Coordinated), fortunately the largest part of our target area belongs to the UTC+0 time zone. Table 1 lists the variables we evaluated in this study.

As for the wind component parameters (*u10*, *v10*, *u100*, *v100*), it is important to note that they represent averages over a model grid box and the native time step of 1 h. In the absence of measurement data, we could not validate the particular reanalysis time series we used, nevertheless in an earlier work [23], a very good agreement was concluded between properly averaged and scaled nacelle anemometer records at a hub height of 65 m and ERA-Interim *u10* and *v10* reanalysis parameters. Since meteorological observations are usually local to a particular point in space and time, differences are present, however they do not affect significantly a statistical evaluation [23]. A recent intercomparison of five reanalysis data banks and tall tower wind observations concluded also that ERA5 surface winds offer the best agreement in correlating and reproducing the observed time evolution and variability [24]. Nevertheless a few times per year, the analysed low level winds (both at 10 m and 100 m), become unrealistically large in particular locations. For example, stored wind speeds at 100 m in the period of January 10, 2018–November 30, 2018 are larger than $4.6 \times 10^4 \text{ms}^{-1}$ therefore it is easy to filter out them as extreme outliers. Point errors (specific grid point at a given time instance) are corrected by linear interpolation.

The geographic region of our work shown in Fig. S1 is located over north-western Africa. The spatial resolution is $0.25^\circ \times 0.25^\circ$, which means 93×101 (lat \times long) grid cells. We examined nearly four decades with a temporal resolution of 3 h, which was enough to represent diurnal variations with a reduced data mass. The four periods were the following: January 01, 1981–12/31/1990; January 01, 1991–12/31/2000; January 01, 2001–12/31/2010; and January 01, 2011–09/31/2018. Since we did not observe any observable differences between the decades in our particular statistical tests, we mostly present results for the last period. The main exception is the full resolution analysis focused into the Sahara (blue rectangle in Fig. S1), where 1 h *ssrd* and $s = \sqrt{u^2 + v^2}$ time series are evaluated in the period of January 01, 2007–09/31/2018 (33×33 grid cells, 102983 data points for each).

The temporal resolutions of 3 h for the whole study area, or 1 h for Western Sahara are not fine enough to consider issues in power system operation (usually based on steps of 15 min). In this respect, our study is a conceptual one based on multi-annual statistical and correlation properties of wind and solar resources.

The parameter *ssrd* (shortwave solar radiation downward) represents the amount of incoming flux of solar radiation on a horizontal unit surface. This parameter comprises both direct and diffuse solar radiation and cloud effects. Radiation from the Sun is partly reflected back to space by clouds and aerosol particles in the atmosphere and some of it is absorbed, the rest is incident on the Earth's surface. To a reasonably good approximation, the parameter *ssrd* is the model equivalent of what would be measured by a pyranometer.

2.1. Spatial correlations of wind fields

In order to characterize spatial correlations of wind speeds between different geographic locations, we determined the Pearson correlation coefficient *R* matrix for each pair of grid points, a matrix of size 9393×9393 . The standard definition of *R* is

$$R_{s_i, s_j} = \frac{\langle [s_i(t) - \overline{s_i(t)}] [s_j(t) - \overline{s_j(t)}] \rangle_t}{\sigma_{s_i} \sigma_{s_j}} \quad (1)$$

where the overline indicate mean value, the nominator is a temporal

mean value of the products and σ is the standard deviation. All calculations were performed in a Python environment (version 3.6) with the standard Numpy and Scipy packages, maps were drawn by the Basemap module.

Pearson correlation is the most common metric for the evaluation of a *linear association* between two time series, see. e.g., Table 1A in Ref. [8]. Its mathematically rigorous foundation requires memory-less Gaussian distributed infinitely long random sequences, none of them is fulfilled by environmental parameters. A somewhat more flexible metric for an evaluation of arbitrary but *monotonous association* between two time series is provided by the Spearman rank correlation coefficient:

$$\rho(s_i, s_j) = \frac{\text{cov}[r(s_i), r(s_j)]}{\sigma_{r_i} \sigma_{r_j}}, \quad (2)$$

which is simply Pearson's correlation coefficient applied to the *ranks* of the observations. Ranks are obtained by an assignment of ordering labels "first" (e.g. largest), "second" (second largest), etc. to a series of observations of a particular variable. This metric was used in a couple of complementarity studies, see Ref. [8], and most recently in Refs. [11, 21].

2.2. Wind electricity estimate

The wind turbine power curve shows the relationship between a wind turbine output power and hub height wind speed [25]. Note that the only purpose of such an operational form is to give a smooth relationship between input speed values and output power based entirely on empirical data; therefore neither the mathematical forms nor the number of parameters are unique [25]. We adopted the following functional form which was proven to provide a reasonable fit for recorded power output data [23,26,27]:

$$P(s) = \begin{cases} a_0(s - s_{ci})^\alpha & \text{if } s_{ci} \leq s \leq s_x \\ \frac{a_1}{1 + \exp[-(s - a_2)^\beta]} & \text{if } s_x < s < s_{co} \\ 0 & \text{if } s < s_{ci}, \text{ and } s > s_{co} \end{cases} \quad (3)$$

Based on Ref. [27], where factory power curves were rescaled simply by the rated power for 6 different turbines and fitted by Eq. (3), the following parameters are used in the model calculations. Cut-in wind speed $s_{ci} = 2.5 \text{ ms}^{-1}$, crossover speed (crossover to the rated power plateau) $s_x = 10.0 \text{ ms}^{-1}$, and cut-out speed $s_{co} = 25.0 \text{ ms}^{-1}$. The further empirical parameters are $a_0 = 0.935$, $\alpha = 2.14$, $a_1 = 100\%$, $a_2 = 9.16 \text{ ms}^{-1}$, and $\beta = 1.05$ (see Fig. 4 in Ref. [27]).

The first equation in the piece-wise nonlinear set (3) reflects the power law dependence of wind power between the cut-in speed s_{ci} and crossover speed s_x . The well-known theoretical value of the exponent is 3, the empirical data of factory power curves reflect somewhat lower values between 2 and 2.5. The second equation between the crossover speed s_x and the cut-out value s_{co} describes the regularized regime by properly rotating the blades. Here the output quickly converges to the nominal peak power resulting in the well known plateau (optimal operating range). The form is a simple logistic function shifted to converge to the rated power.

2.3. Combined solar and wind electricity estimate

As for an estimate of solar power alone, we use the following considerations. The electric output power of a photovoltaic (PV) panel depends linearly on the incoming flux of the solar radiation. It is a trivial fact that an optimal positioning of a PV panel is not horizontal away from the equator, it should be properly tilted to receive more direct and less grazing incidence radiation. Jacobson and Jadhav [28] determined globally an optimal tilt angle and insolation gain relative to horizontal for all countries of the world. Considering our test area centered in the In Salah region, Sahara, at the northern edge (33°N) the optimal tilt angle

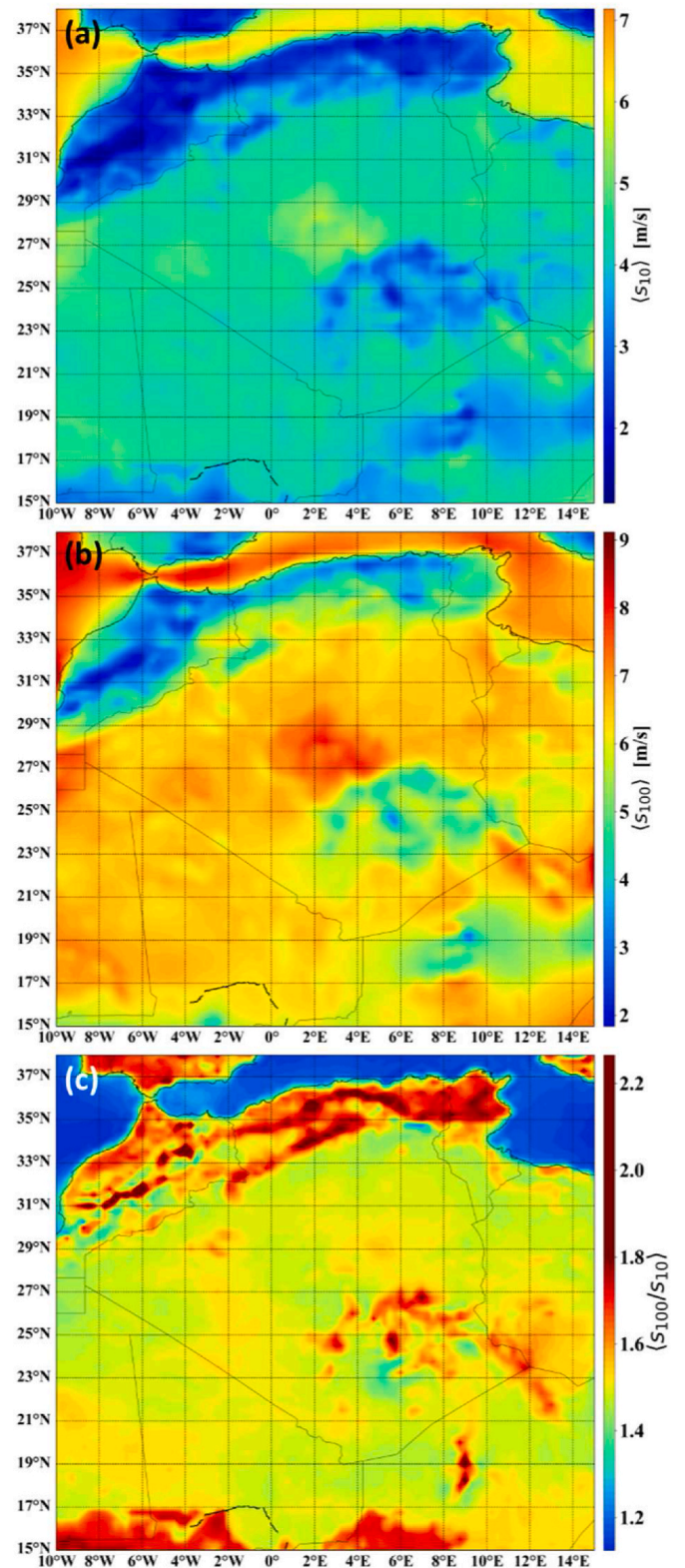


Fig. 1. Geographic distribution of mean wind speed (a) at 10 m, and (b) at 100 m altitude. Note the different color scales. (c) Temporal mean of instantaneous wind speeds ratio s_{100m}/s_{10m} . The evaluated period is from 01/01/2011 to 09/31/1998.

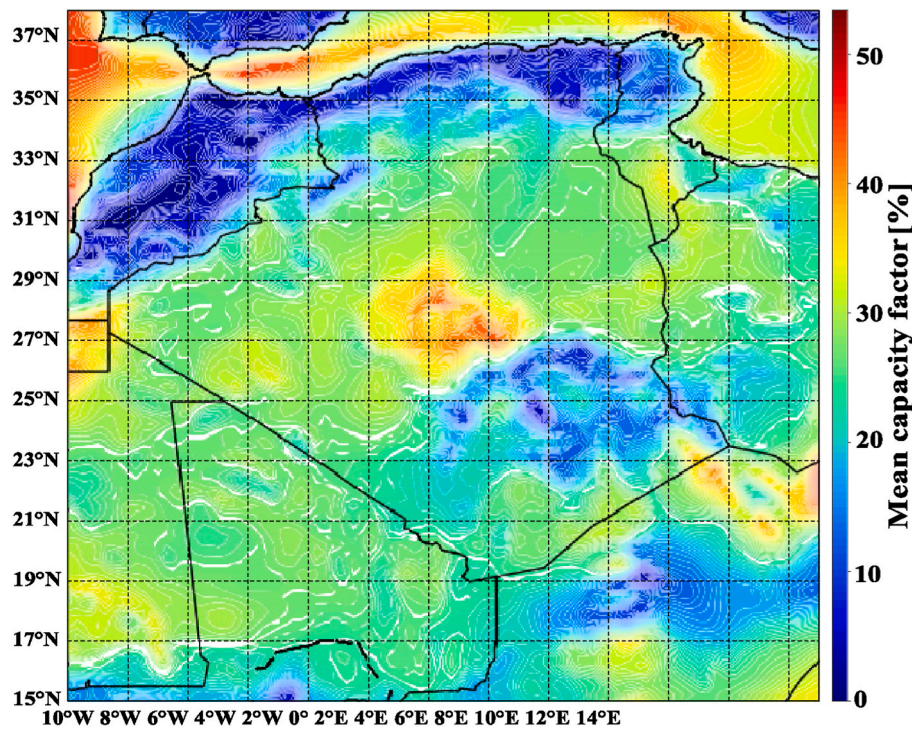


Fig. 2. Geographic distribution of the mean capacity factor in the period of 01/01/2011–09/31/2018 (percentage values).

of fixed PV panels is around 28–29°, while at the southern edge (25°N) the optimum is around 24–26° (see Fig. 2 in Ref. [28]). Accordingly, the gain of short wave radiation flux is a factor between 1.10 and 1.15, see Fig. 5b in Ref. [28]. We use this correction factor by estimating PV output power as a function of downward solar radiation flux $ssrd$. Note that the optimal tilt angle and azimuth of a PV panel change hour by hour following the daily solar cycle and seasonal variation of the elevation of the Sun. However, such Sun-tracking mechanisms are expensive and demanding steady maintenance, therefore we consider the common compromise of fixing the tilt and azimuth (southern direction) which results in the maximal annual mean output [28].

Other known small corrections (e.g. the temperature of the PV panel, possible cloud shadowing, dust cover etc.) are omitted. Nevertheless, dust cover might be a serious issue in the Sahara. Several studies concluded that accumulation of dust on the surface of photovoltaic cells causes a significant degradation of electricity generation [29–31]. A recent experimental study [31] found that a sand cover of 100 gm^{-2} decreases the output power by $\sim 12\%$, however a weekly dry cleaning (brushes and clothes) reduces the power loss to less than 1%.

The simplest model of an aggregated output of solar and wind electricity P_{tot} as a function of time t consists of a single parameter, the resource fraction $0 \leq c \leq 1$ which is the ratio of wind and solar contribution to a total rated power of 100% (see e.g., Ref. [27]):

$$P_{tot}(t) = c \times P_{wind}(t) + (1 - c) \times 0.1 \times 1.125 \times ssrd(t) \quad (4)$$

Here the coefficient 0.1 on the right hand side follows from the practice that the rated output power (100%) of a solar panel is determined at 1000 Wm^{-2} perpendicular insolation and at a panel temperature of 25°C, but we neglect temperature effects here. The factor 1.125 is simply the mean gain of insolation at optimal tilt angles, as discussed above. The wind power output $P_{wind}(t)$ is estimated by transforming the wind speed $s_{100}(t)$ with Eq. (3). The two limiting values $c = 0$ and $c = 1$ belong to pure solar and pure wind electricity generation.

3. Results

3.1. Mean wind speeds and capacity factors

Fig. 1 presents the mean wind speeds determined over almost 8 years with a resolution of 3 h. Fig. 1b reveals that mean Saharan wind speeds at an altitude of 100 m are comparable with the values over open sea areas, both over the Mediterranean Sea and the Atlantic Ocean. Fig. 1c suggests that the reason is a steeper vertical wind profile over the desert, the ratios s_{100m}/s_{10m} are substantially larger (1.5–1.6) than over the open sea (1.1–1.2). It is an interesting fact that the highest wind speed ratios are obtained close to the coastal areas at the north. This areas strongly overlap with the regions covered by low and high vegetation (see Fig. S1) resulting in low surface wind speeds (Fig. 1a). Similarly, wind speed mean ratios are large over the southern belt of low vegetation cover (red coloring in Fig. 1c), nevertheless the dampening at the surface at these locations is so strong (blue coloring in Fig. 1a) that even a factor 2.0–2.2 means low mean values at 100 m (blue-green coloring in Fig. 1b).

The relatively large hub-height mean wind speeds at 100 m over the Saharan region suggest that the capacity factors of wind electricity generation should be comparable with off-shore wind farms. The capacity factor is simply the ratio of total realized output and rated output for an extended period, usually 1 year. It is given either as a dimensionless number between 0 (no electricity output) and 1 (continuous full capacity output) or as a percentage value between 0 and 100%. We adopted the latter notation. Indeed, Fig. 2 reveals that capacity factors larger than 40–45% are expected particularly over the central region of Algeria (roughly in Salah province). Here the wind speeds s_{100} are transformed by Eq. (3) as described above. Minimal capacity factor values are obviously located in the middle of the low wind belt in Morocco (see also Fig. 1a and b). The value is less than 1% in the region of Al Haouz, particularly around 31.25°N (lat), 8.0°W (lon). The practically windless area is located north-west behind the Atlas Mountains. (Notably, Morocco has a much larger off-shore than on-shore wind energy potential [32].) The situation is similar over the densely populated coastal regions in Algeria, unfortunately the low expected capacity

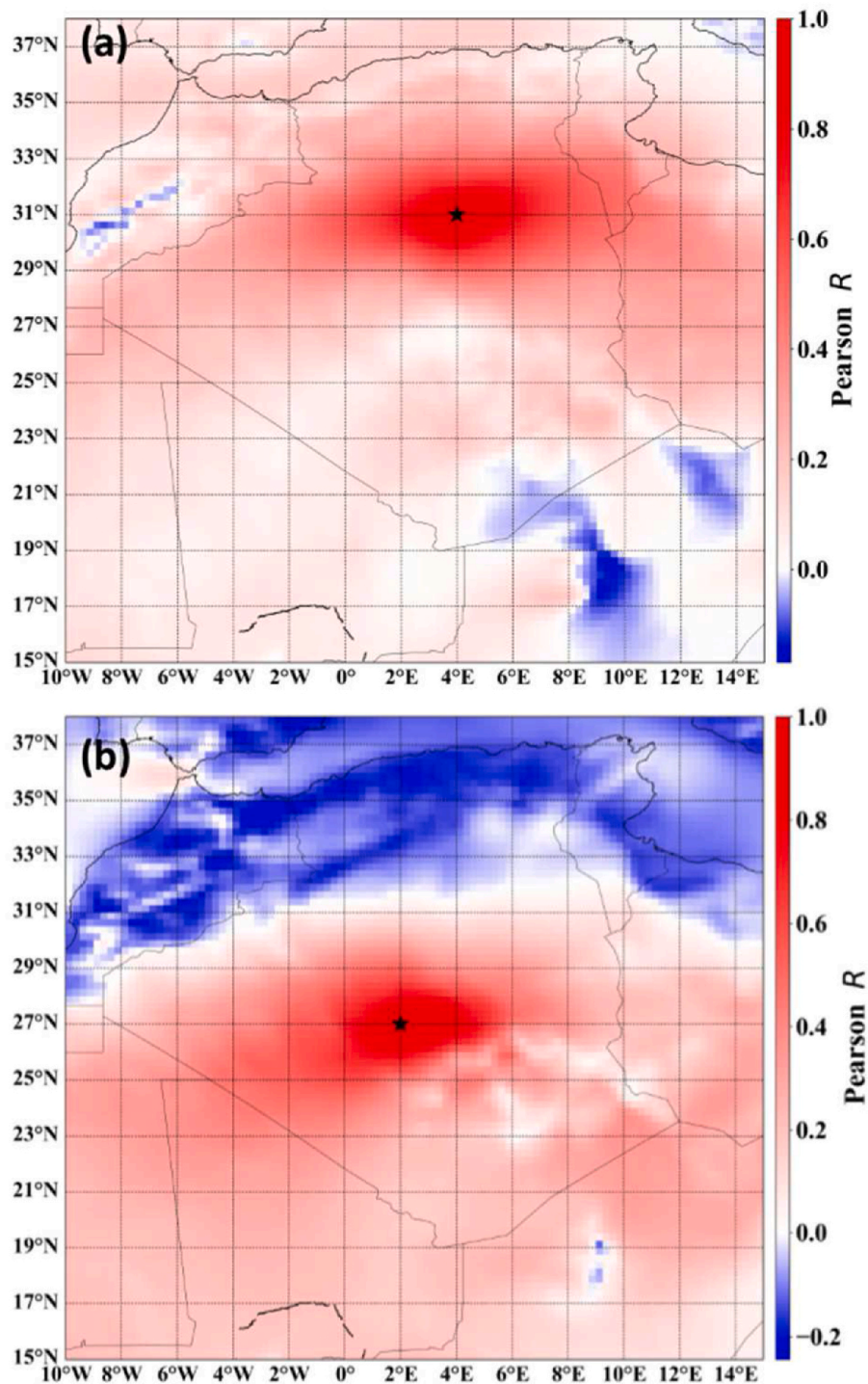


Fig. 3. Geographic distribution of the Pearson correlation coefficient R between the target location (black symbol) and all the other grid cells. 100 m wind speed records are evaluated in the interval 01/01/2011 - 10/31/2018. (a) Target location 31°N, 4°E (~120 km north-east from the oasis town El Menia, Algeria); (b) 27°N, 2°E (~14 km south-east from the town In Ghar, Algeria). Note that the color scales are strongly asymmetric.

factors question any reasonable installation of wind turbines.

3.2. Spatial correlations of wind speeds

Spatial wind speed correlations can be an essential factor prior to a wind farm installation, especially when wind electricity is integrated into an extended grid. The quality of an aggregated output can be dramatically improved when the output of wind farms located on sites of large negative correlations (anti-correlations) are integrated. In order to

check the potential of such distributed installation, we determined the Pearson correlation coefficient R by Eq. (1) between all the 93×101 grid-points, as described in Subsection 2.1.

The result is the correlation matrix of size 9393×9393 , which permits to determine the correlation map for each geographic location. Examples are shown in Fig. 3a and b for two Saharan locations (further two examples are in Fig. S2). All maps demonstrate that spatial correlations are very strong over the desert, similarly to open sea surfaces. The patterns are rather complex, therefore the usual characterization by

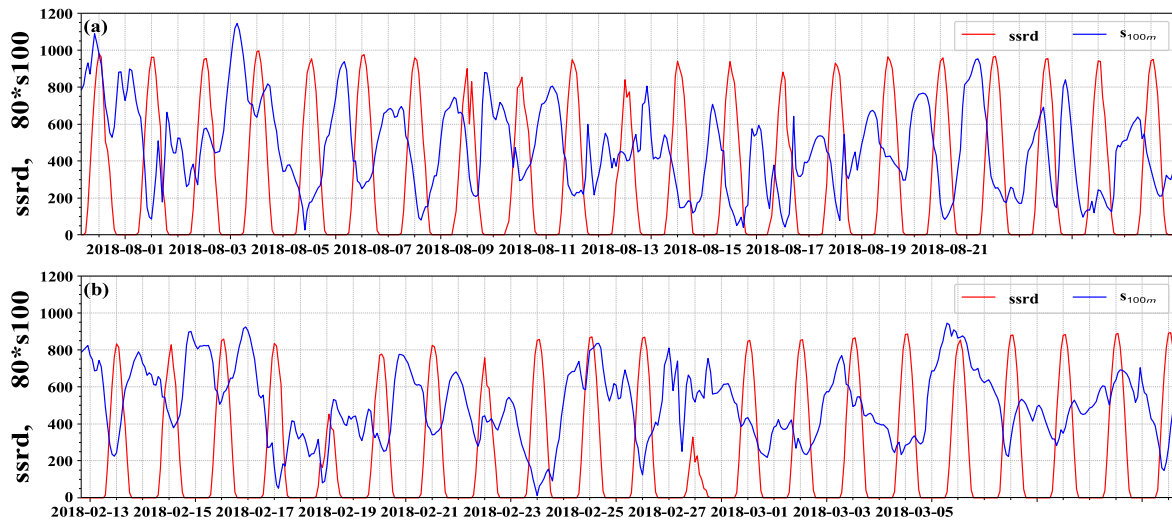


Fig. 4. Time series of downward solar radiation flux at the surface (in units of Wm^{-2} , red) and 100 m wind speed (ms^{-1} , blue) multiplied by 80 for the sake of visualization. 500–500 h are plotted (about 3 weeks). (a) Location 27°N , 0° (10 km south-east from the town Sali, Algeria), August 2018; (b) 27°N , 2°E (14 km south-east from the town In Ghar, Algeria), February 2018.

a single correlation length (assuming an exponential decay) is an oversimplification (see Ref. [33] and references therein). For example, in Fig. 3a very strong spatial correlations ($R = 1$) extend at least $\pm 4^{\circ}$ (± 380 km) in the zonal direction along 31°N latitude, while the meridional decay along 4°E longitude is faster ($\pm 2^{\circ}$, ± 222 km). The pattern of strong positive correlations in Fig. 3b is asymmetric in the zonal direction, nevertheless the characteristic lengths of strong correlations in any direction are over 200 km. Strong correlations are expected over the Sahara after inspecting the instantaneous or mean wind fields. Fig. S3a illustrates a nighttime (at 03:00 UTC), while Fig. S3b a daytime (at 15:00 UTC) mean flow fields, where vectorial mean of 100 m wind velocities are calculated and visualized. Indeed, the flow fields exhibit very large coherent structures, particularly over the Sahara. Such wind velocity patterns are strongly related to the continental scale westward and northward dust transport [34,35].

Fig. 3b (and Figs. S2, S3) illustrate another general feature of spatial correlations: for most of the grid-cells, weak anti-correlations appear for very large distances. The smallest negative correlation found is around $R = -0.25$ for a few locations, and in general, places of low wind and high wind regions are anti-correlated as in Fig. 3b. By inspecting a large number of such correlation maps, we can conclude that the exploitation of negative spatial correlations in an aggregated wind electricity production is not realistic over this geographic area.

Note that the consideration of Spearman rank correlation [Eq. (2)] leads to the same conclusion, correlation maps are almost identical (see Supporting Figs. 2 and 3).

3.3. Combined wind-solar electricity production

An obvious renewable resource in desert areas is photovoltaic electricity generation. We evaluated the possible role of *ssrd* (surface solar radiation downward) in an energy portfolio. The geographic distribution of long time mean *ssrd* values is exhibited in Fig. S4, Supporting Material. Particularly, we analysed the potential of aggregated wind-solar electricity production over the middle of Saharan region in Algeria (see Fig. S1), where the expected capacity factors for wind electricity generation are the highest (see Fig. S5 for mean wind speeds over this area).

The simple model construction described in Subsection 2.3 is an upper limit, losses and other disturbing factors (warming of solar cells, dust cover, etc.) are not considered here. The linear combination of the two terms given by Eq. (4) means that the total output integrated over a

longer period is a linear function of the resource fraction c , where the slope is determined by the capacity factors of pure wind and pure solar generation. When the former is larger, the slope of the line is negative, in the opposite case the slope is positive.

Fig. 4 illustrates a peculiar feature of *ssrd* and s_{100} hourly time series inside the western Saharan region (blue rectangle in Fig. S1). It is apparent that desert wind intensifies quiet often during the night periods. The examples shown are not cherry picking, this is the general tendency in this geographic region, and in every seasons. The numerical values of the correlation coefficient R are rather moderate ($R > -0.3$), however this is the consequence of the very large standard deviation of *ssrd* in the denominator of Eq. (1). Indeed, downward solar radiation varies each day between zero and $800\text{--}1000 \text{ Wm}^{-2}$, even in the northern edge of the region (33°N) is not less than 600 Wm^{-2} in the middle of the winter season.

When the main goal is to maximize renewable electricity production, the solution is simple: choose the resource which has the higher total capacity factor. The largest part of the Saharan region "solar-dominated", therefore maximum production can be achieved by pure photovoltaic generation. The price is the strong oscillation, there is zero production during the nights. (Unfortunately, industrial scale renewable energy storage is not a option in Africa, because all known technology require very large investment capital [36]).

When the target of optimization is a smoother production, it is worth to consider the possible role of nighttime desert winds. One possible parameter to characterize the strength of fluctuations for a given time series is the *coefficient of variation* (CV) which is simply the ratio of *standard deviation* and the *long-time mean value*. We determined systematically CV as a function of resource fraction c [see Eq. (4)], and found that it has a unique minimum value (see Fig. 5a-inset) defining an optimal combination ratio c_{opt} with the smoothest possible output. Fig. 5a illustrates that this optimum is between 0.56 and 0.69 (P_{wind} proportion) depending on the particular location. At the optimal value of resource combination c_{opt} , the total output is obviously less than the maximum, therefore we determined the total capacity factor loss for each gridcell, which is the difference [$P_{tot}(c_{opt}) - P_{tot}(c_{max})$]. [Note again that c_{max} is either 0 or 1 for solar-dominated or wind-dominated locations, see Eq. (4).] The result is shown in Fig. 5b. The large blue areas indicate that the capacity factor loss is only a few percent at the optimal resource combination c_{opt} for most locations.

The coefficient of variation CV shown in Fig. 5a-inset has very substantial drop at several places around c_{opt} , nevertheless one can

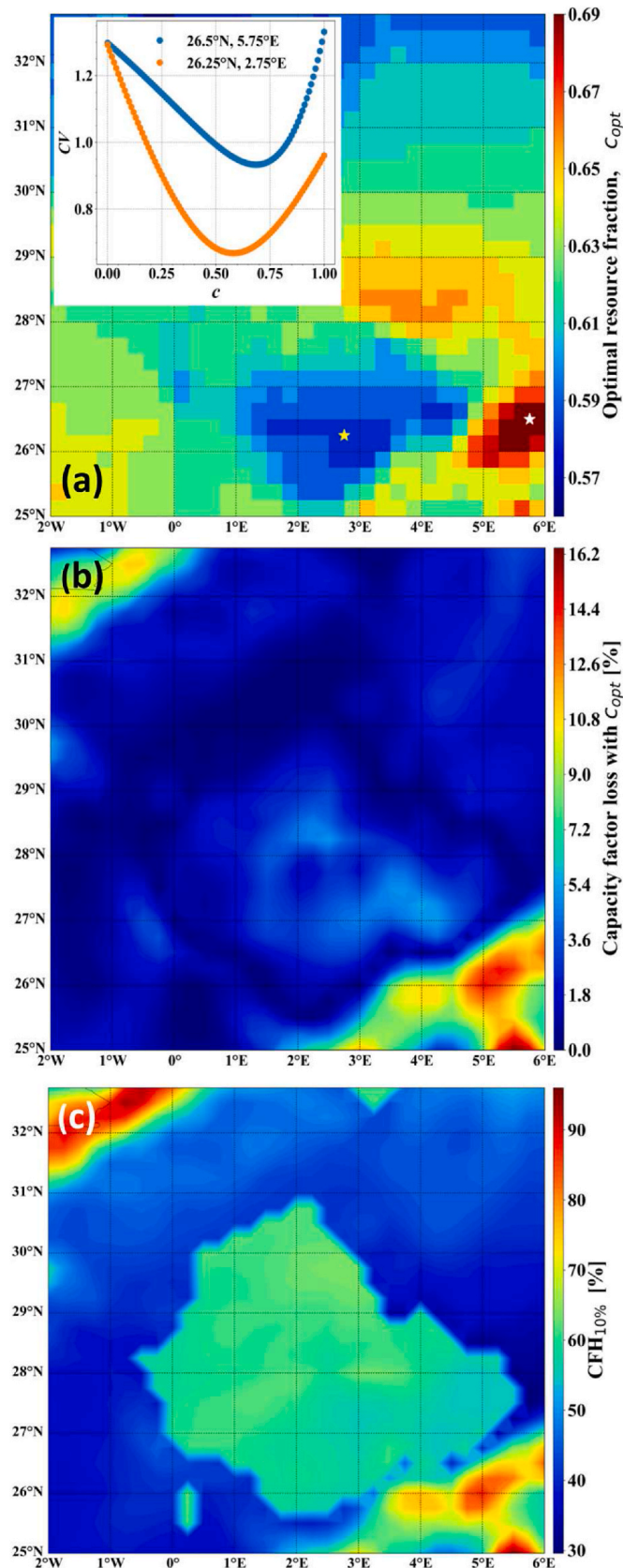


Fig. 5. (a) Geographic distribution of optimal resource fraction c_{opt} , where the coefficient of variation CV is minimal. The inset illustrates the CV (c) dependence for two sites: 26.5°N , 5.75°E (white star), and 26.25°N , 2.75°E (yellow star). (b) Capacity factor loss with the optimal resource fraction c_{opt} relative to the maximum value. (c) The ratio $CFH_{10\%}$, its explanation is in the text.

demonstrate the improvement of the combined output power quality in more transparent ways. As an example, we determined the ratio of total time when the output is less than 10% at c_{opt} over the total time when the output is less than 10% at c_{max} , denoted by $CFH_{10\%}$ (Capacity Factor Hiatus). The geographic distribution of $CFH_{10\%}$ is shown in Fig. 5c. The blueish areas exhibit a dramatic improvement, the total time of low aggregated output at the optimal resource ratio c_{opt} is only 30–40% relative to the maximal output at c_{max} . The huge green island in the middle of the region unambiguously identifies the wind-dominated locations ($c_{max} = 1$), blue sites are solar-dominated ($c_{max} = 0$). The reason of the dampened improvement over wind-dominated areas ($CFH_{10\%} = 60\%$) is simply the fact that the wind speeds at 100 m almost never drop to zero, still the incorporation of solar electricity generation provides a much better quality aggregated output. The improvement over solar-dominated locations (blue in Fig. 5c) is more pronounced because any inclusion of nighttime wind electricity production immediately shortens the periods of zero output.

4. Discussion

Previous assessments of wind energy potential over Algeria have been mostly based on surface measurements of meteorological stations or reanalysis wind fields at 10 m standard height and common extrapolation methodologies to estimate wind strengths at assumed hub-heights of 80–100 m. The list of most relevant studies and their key features are the following: Merzouk [37], 10 years, 64 weather stations, annual wind map; Djamaï and Merzouk [38] wind farm potential at around Ardar, 5 years of WASP data; Stambouli et al. [39], overview of Algeria's whole energy sector, particular emphasize on renewable resource potentials; Boudia et al. [40], 5 years, 87 weather stations, wind maps at 10 m height; Daaou Nedjari et al. [41], 10 years, 95 weather stations, probability distributions, wind maps for 10 m and 80 m (extrapolated); Boudia and Santos [42], 33 years of ERA Interim data, validation by 42 ground stations for 2014, probability distributions, regional wind resource maps; Ounis and Aries [43], 17 years of ERA Interim data, evaluation of various probability distributions; most recently Guezgouz et al. [11], solar and wind energy complementarity in Algeria for the year 2019 with 1 h temporal resolution, wind data from MERRA-2 reanalysis (10 m, extrapolated), insolation data from CAMS reanalysis. The wind maps are similar to our Fig. 1a, however maximum mean values are shifted somewhat westward, around Adrar (27.87°N , 0.28°W). The wind maps by Nedjari et al. in Ref. [41] (Fig. 3 for 10 m and Fig. 5 for 80 m) and Guezgouz et al. [11] exhibit a good agreement with ours, windiest places are centered around In Salah (27.18°N , 2.48°E).

All the above listed studies are based on wind fields at the 10 m standard height, and extrapolations are used for higher altitudes. However, extrapolation of 10 m wind speeds to 100 m by e.g., the usual power law approximation may result in erroneous results. A particularly spectacular example is presented in Supplementary Fig. 2 by Sterl et al. [7]. The mean daily cycle of surface wind (thus the extrapolated speed too) exhibits an enhancement during the daylight periods, nevertheless ERA5 100 m wind speeds have the very opposite tendency of an enhancement during the nights.

As for the recent resource compatibility study by Guezgouz et al., they also use reanalysis data (MERRA-2 and CAMS) of high temporal resolution for the year of 2019. The spatial resolution is somewhat lower ($0.5^\circ \times 0.5^\circ$), and 10 m wind speeds are extrapolated by the common power law with the exponent of $1/7$. There is no energy mix in the study, the Spearman correlation coefficient Eq. (2) is used as a complementarity index. Still, they found similar daily anti-correlations between solar and wind resources at around the same locations as we obtained.

We think that our simple model framework of electricity integration scheme by Eq. (4), the characterization of the output quality by the coefficient of variation (CV) and by the capacity factor loss at an optimal

combination ratio (Fig. 5b) or the capacity factor hiatus (CFH_{10%}, Fig. 5c) provide a quick and transparent methodology to identify suitable geographic locations, where installation of combined wind and solar electricity systems are promising.

Declaration of competing interest

The authors declare that they have no known competing financial interests or personal relationships that could have appeared to influence the work reported in this paper.

Acknowledgements

The work of KM is supported by the Stipendium Hungaricum Scholarship of the Tempus Public Foundation. MV is supported by the János Bolyai Research Scholarship of the Hungarian Academy of Sciences, the National Research, Development and Innovation Office (NKFIH) [grant numbers FK125024 and K125171], and by the ÚNKP-18-4 New National Excellence Program of the Ministry of Human Capacities of Hungary. IMJ thanks for the support by the Max-Planck Institute for the Physics of Complex Systems.

Appendix A. Supplementary data

Supplementary data to this article can be found online at <https://doi.org/10.1016/j.rser.2021.111558>.

Credit author statement

Imre M. Jánosi: Conceptualization of this study; Methodology; Validation; Writing - original draft. Karim Medjdoub: Investigation; Software; Visualization. Miklós Vincze: Investigation; Validation; Writing - review and editing.

References

- McCollum DL, Echeverri LG, Busch S, Pachauri S, Parkinson S, Rogelj J, et al. Connecting the sustainable development goals by their energy inter-linkages. *Environ Res Lett* 2018;13:033006. <https://doi.org/10.1088/1748-9326/aaaf3>.
- Ouedraogo NS. Opportunities, barriers and issues with renewable energy development in Africa: a comprehensive review. *Curr Sustainable Renew Energy Rep* 2019;6:52–60. <https://doi.org/10.1007/s40518-019-00130-7>.
- Longa FD, van der Zwaan B. Heart of light: an assessment of enhanced electricity access in Africa. *Renew Sustain Energy Rev* 2021;136:110399. <https://doi.org/10.1016/j.rser.2020.110399>.
- United Nations. The sustainable development goals report. 2020. accessed 2 Nov. 2020, <https://unstats.un.org/sdgs/report/2020/>. 2020. Online.
- López-Ballesteros A, Beck J, Helmschrot J, Saunders M. Harmonised observations of climate forcing across Africa: an assessment of existing approaches and their applicability. *Environ Res Lett* 2020;15:075003. <https://doi.org/10.1088/1748-9326/ab82ce>.
- Engeland K, Borga M, Creutin JD, François B, Ramos MH, Vidal JP. Space-time variability of climate variables and intermittent renewable electricity production – a review. *Renew Sustain Energy Rev* 2017;79:600–17. <https://doi.org/10.1016/j.rser.2017.05.046>.
- Sterl S, Liersch S, Koch H, van Lipzig NPM, Thiery W. A new approach for assessing synergies of solar and wind power: implications for west africa. *Environ Res Lett* 2018;13:094009. <https://doi.org/10.1088/1748-9326/aad8f6>.
- Jurasz J, Canales F, Kies A, Guezgouz M, Beluco A. A review on the complementarity of renewable energy sources: concept, metrics, application and future research directions. *Sol Energy* 2020;195:703–24. <https://doi.org/10.1016/j.solener.2019.11.087>.
- Solomon A, Child M, Caldera U, Breyer C. Exploiting wind-solar resource complementarity to reduce energy storage need. *AIMS Energy* 2020;8(5):749–70. <https://doi.org/10.3934/ENERGY.2020.5.749>.
- Weschenfelder F, de Novaes Pires Leite G, Araújo da Costa AC, de Castro Vilela O, Ribeiro CM, Villa Ochoa AA, et al. A review on the complementarity between grid-connected solar and wind power systems. *J Clean Prod* 2020;257:120617. <https://doi.org/10.1016/j.jclepro.2020.120617>.
- Guezgouz M, Jurasz J, Chouai M, Bloomfield H, Bekkouche B. Assessment of solar and wind energy complementarity in Algeria. *Energy Convers Manag* 2021;238:114170. <https://doi.org/10.1016/j.enconman.2021.114170>.
- Prasad AA, Taylor RA, Kay M. Assessment of solar and wind resource synergy in Australia. *Appl Energy* 2017;190:354–67. <https://doi.org/10.1016/j.apenergy.2016.12.135>.
- Sahin AZ. Applicability of wind-solar thermal hybrid power systems in the northeastern part of the Arabian Peninsula. *Energy Sources* 2000;22(9):845–50. <https://doi.org/10.1080/009083100300001645>.
- Heide D, von Bremen L, Greiner M, Hoffmann C, Speckmann M, Bofinger S. Seasonal optimal mix of wind and solar power in a future, highly renewable Europe. *Renew Energy* 2010;35(11):2483–9. <https://doi.org/10.1016/j.renene.2010.03.012>.
- Zappa W, van den Broek M. Analysing the potential of integrating wind and solar power in Europe using spatial optimisation under various scenarios. *Renew Sustain Energy Rev* 2018;94:1192–216. <https://doi.org/10.1016/j.rser.2018.05.071>.
- Widen J. Correlations between large-scale solar and wind power in a future scenario for Sweden. *IEEE Trans Sustain Energy* 2011;2:177–84. <https://doi.org/10.1109/TSTE.2010.2101620>.
- Jerez S, Trigo R, Sarsa A, Lorente-Plazas R, Pozo-Vázquez D, Montávez J. Spatio-temporal complementarity between solar and wind power in the Iberian Peninsula. *Energy Procedia* 2013;40:48–57. <https://doi.org/10.1016/j.egypro.2013.08.007>.
- Santos-Alamillos F, Pozo-Vázquez D, Ruiz-Arias J, Von Bremen L, Tovar-Pescador J. Combining wind farms with concentrating solar plants to provide stable renewable power. *Renew Energy* 2015;76:539–50. <https://doi.org/10.1016/j.jrenene.2014.11.055>.
- Guozden T, Carbajal JP, Bianchi E, Solarte A. Optimized balance between electricity load and wind-solar energy production. *Front Energy Res* 2020;8:16. <https://doi.org/10.3389/fenrg.2020.00016>.
- Liu L, Wang Z, Wang Y, Wang J, Chang R, He G, et al. Optimizing wind/solar combinations at finer scales to mitigate renewable energy variability in China. *Renew Sustain Energy Rev* 2020;132:110151. <https://doi.org/10.1016/j.rser.2020.110151>.
- Jurasz J, Mikulík J, Dqbek PB, Guezgouz M, Kazmierczak B. Complementarity and 'resource droughts' of solar and wind energy in Poland: an era-5-based analysis. *Energies* 2021;14(4):1118. <https://doi.org/10.3390/en14041118>.
- Hersbach H, Bell B, Berrisford P, Hirahara S, Horányi A, Muñoz-Sabater J, et al. The ERA5 global reanalysis. *Q J R Meteorol Soc* 2020;146:1999–2049. <https://doi.org/10.1002/qj.3803>.
- Kiss P, Varga L, Jánosi IM. Comparison of wind power estimates from the ECMWF reanalyses with direct turbine measurements. *J Renew Sustain Energy* 2009;1:033105. <https://doi.org/10.1063/1.3153903>.
- Ramon J, Lledó L, Torralba V, Soret A, Doblas-Reyes FJ. What global reanalysis best represents near-surface winds? *Q J R Meteorol Soc* 2019;145:3236–51. <https://doi.org/10.1002/qj.3616>.
- Lydia M, Kumar SS, Selvakumar AI, Kumar GEP. A comprehensive review on wind turbine power curve modeling techniques. *Renew Sustain Energy Rev* 2014;30:452–60. <https://doi.org/10.1016/j.rser.2013.10.030>.
- Kiss P, Jánosi IM. Limitations of wind power availability over Europe: a conceptual study. *Nonlinear Process Geophys* 2008;15(6):803–13. <https://doi.org/10.5194/npg-15-803-2008>.
- Jánosi IM. Model study of combined wind and solar electricity production in Hungary. *J Renew Sustain Energy* 2013;5:033102. <https://doi.org/10.1063/1.4803528>.
- Jacobson MZ, Jadhav V. World estimates of PV optimal tilt angles and ratios of sunlight incident upon tilted and tracked PV panels relative to horizontal panels. *Sol Energy* 2018;169:55–66. <https://doi.org/10.1016/j.solener.2018.04.030>.
- Fountoukis C, Figgis B, Ackermann L, Ayoub MA. Effects of atmospheric dust deposition on solar PV energy production in a desert environment. *Sol Energy* 2018;164:94–100. <https://doi.org/10.1016/j.solener.2018.02.010>.
- Pulipaka S, Kumar R. Analysis of soil distortion factor for photovoltaic modules using particle size composition. *Sol Energy* 2018;161:90–9. <https://doi.org/10.1016/j.solener.2017.11.041>.
- Alnasser TM, Mahdy AM, Abass KI, Chaichan MT, Kazem HA. Impact of dust ingredient on photovoltaic performance: an experimental study. *Sol Energy* 2020;195:651–9. <https://doi.org/10.1016/j.solener.2019.12.008>.
- Soares PMM, Lima DCA, Semedo A, Cabos W, Sein DV. Climate change impact on Northwestern African offshore wind energy resources. *Environ Res Lett* 2019;14:124065. <https://doi.org/10.1088/1748-9326/ab5731>.
- Ren G, Wan J, Liu J, Yu D. Spatial and temporal correlation analysis of wind power between different provinces in China. *Energy* 2020;191:116514. <https://doi.org/10.1016/j.energy.2019.116514>.
- Lamancusa C, Wagstrom K. Global transport of dust emitted from different regions of the Sahara. *Atmos Environ* 2019;214:116734. <https://doi.org/10.1016/j.atmosenv.2019.05.042>.
- Koren I, Kaufman YJ, Washington R, Todd MC, Rudich Y, Martins JV, et al. The Bodélé depression: a single spot in the Sahara that provides most of the mineral dust to the Amazon forest. *Environ Res Lett* 2006;1:014005. <https://doi.org/10.1088/1748-9326/1/1/014005>.
- Krishan O, Suhag S. An updated review of energy storage systems: classification and applications in distributed generation power systems incorporating renewable energy resources. *Int J Energy Res* 2019;43(12):6171–210. <https://doi.org/10.1002/er.4285>.
- Merzouk NK. Wind energy potential of Algeria. *Renew Energy* 2000;21(3):553–62. [https://doi.org/10.1016/S0960-1481\(00\)00090-2](https://doi.org/10.1016/S0960-1481(00)00090-2).
- Djamai M, Merzouk NK. Wind farm feasibility study and site selection in Adrar, Algeria. *Energy Procedia* 2011;6. <https://doi.org/10.1016/j.egypro.2011.05.016>.
- Stambouli AB, Khait Z, Flazi S, Kitamura Y. A review on the renewable energy development in Algeria: current perspective, energy scenario and sustainability issues. *Renew Sustain Energy Rev* 2012;16(7):4445–60. <https://doi.org/10.1016/j.rser.2012.04.031>.

- [40] Boudia SM, Benmansour A, Tabet Hellal MA. Wind resource assessment in Algeria. *Sustain Cities Soc* 2016;22:171–83. <https://doi.org/10.1016/j.scs.2016.02.010>.
- [41] Daaou Nedjari H, Haddouche SK, Balehouane A, Guerri O. Optimal windy sites in Algeria: potential and perspectives. *Energy* 2018;147:1240–55. <https://doi.org/10.1016/j.energy.2017.12.046>.
- [42] Boudia SM, Santos JA. Assessment of large-scale wind resource features in Algeria. *Energy* 2019;189:116299. <https://doi.org/10.1016/j.energy.2019.116299>.
- [43] Ounis H, Aries N. On the wind resource in Algeria: probability distributions evaluation. *P I Mech Eng A - J Pow* 2020;235(5):1187–204. <https://doi.org/10.1177/0957650920975883>.